

Comparative analysis of muon-capture and $0\nu\beta\beta$ -decay matrix elements

L. Jokiniemi  and J. Suhonen 

Department of Physics, University of Jyväskylä, P. O. Box 35 (YFL), FI-40014, Finland



(Received 24 January 2020; revised 26 March 2020; accepted 30 June 2020; published 3 August 2020)

Average matrix elements of ordinary muon capture (OMC) to the intermediate nuclei of neutrinoless double beta ($0\nu\beta\beta$) decays of current experimental interest are computed and compared with the corresponding energy and multipole decompositions of $0\nu\beta\beta$ -decay nuclear matrix elements (NMEs). The present OMC computations are performed using the Morita-Fujii formalism by extending the original formalism beyond the leading order. The $0\nu\beta\beta$ NMEs include the appropriate short-range correlations, nuclear form factors, and higher-order nucleonic weak currents. The nuclear wave functions are obtained in extended no-core single-particle model spaces using the spherical version of the proton-neutron quasiparticle random-phase approximation with two-nucleon interactions based on the Bonn one-boson-exchange G matrix. Both the OMC and $0\nu\beta\beta$ processes involve 100-MeV-range momentum exchanges and hence similarities could be expected for both processes in the feeding of the $0\nu\beta\beta$ intermediate states. These similarities may help improve the accuracy of the $0\nu\beta\beta$ NME calculations by using the data from the currently planned OMC experiments.

DOI: [10.1103/PhysRevC.102.024303](https://doi.org/10.1103/PhysRevC.102.024303)

I. INTRODUCTION

Ordinary muon capture (OMC) is a process in which a negative muon from an atomic K orbit is captured by the nucleus of the atom. The large mass of the captured muon induces large momentum exchange, $q \approx 50\text{--}100$ MeV, which leads to final states that are both highly excited and of high multipolarity. These same states are expected to contribute as the intermediate states of neutrinoless double beta ($0\nu\beta\beta$) decay in $0\nu\beta\beta$ decay chains. Here, we discuss cases where the OMC happens on the daughter nucleus of a $0\nu\beta\beta$ -decay parent and hence the OMC corresponds to the right virtual branch (β^+ type of transitions) of the $0\nu\beta\beta$ decay. This makes OMC a promising tool to study the nuclear matrix elements (NMEs) of the $0\nu\beta\beta$ decay [1,2].

We are interested in the ground-state-to-ground-state $0\nu\beta\beta$ decay, which can be schematically written as

$${}_{Z-2}^A X'(0^+) \dashrightarrow {}_{Z-1}^A Y(J^\pi) \dashrightarrow 2e^- + {}_Z^A X(0^+), \quad (1)$$

where the even-even parent nucleus X' of mass number A and atomic number $Z - 2$ in its 0^+ ground state emits two electrons e^- leading to the 0^+ ground state of its daughter X , an even-even isobar of atomic number Z . The transition goes through the virtual states of multipolarity J^π of the intermediate odd-odd nucleus Y of atomic number $Z - 1$; here, J is the angular momentum and π the parity of the intermediate state. The dashed arrow represents virtual transitions through the intermediate states. Using the notation of Eq. (1) the OMC process, which corresponds to the right branch of the $0\nu\beta\beta$ process of Eq. (1), can be illustrated as

$$\mu^- + {}_Z^A X(0^+) \rightarrow \nu_\mu + {}_{Z-1}^A Y(J^\pi), \quad (2)$$

where the muon (μ^-) is captured by the 0^+ ground state of the even-even nucleus X leading to the J^π multipole states of

its odd-odd isobar Y (see the review by Measday [3]). At the same time a muon neutrino ν_μ is emitted. Comparing Eqs. (1) and (2) one can see how ordinary muon capture is linked with neutrinoless double β decay: OMC feeds the same excited J^π states of Y that are involved as virtual states in the $0\nu\beta\beta$ decay.

Through the years a number of calculations for the OMC transitions in different nuclear-structure formalisms and for various nuclei have been performed in order to probe the right-leg virtual transitions of $0\nu\beta\beta$ decays as well as the value of the particle-particle interaction parameter g_{pp} of the proton-neutron quasiparticle random-phase approximation (pnQRPA) [4–6], or the in-medium renormalization of the axial-vector coupling constant g_A [7–12]. Thanks to the large momentum exchange in the OMC, the process activates also the induced weak currents, including the weak magnetism and pseudoscalar contributions, quite like in the case of the $0\nu\beta\beta$ decay [13]. The magnitude of the induced pseudoscalar term is mostly unknown in atomic nuclei [7,8,14–21]. Additional OMC experiments and calculations concerning nuclei involved in $0\nu\beta\beta$ decays could help theories better understand the possible connections between OMC and $0\nu\beta\beta$ NMEs as well as the effective values of the weak couplings [22].

There have been early attempts to compare the OMC rates against the $2\nu\beta\beta$ (two-neutrino double beta decay) NMEs for light nuclei using the nuclear shell model [6]. In the work of Kortelainen *et al.* [6] it was found that there was a clear correlation between the energy distributions of the OMC rates to 1^+ states and the energy decomposition of the $2\nu\beta\beta$ NMEs for the $2\nu\beta\beta$ decays of the sd -shell nuclei ^{36}Ar , ^{46}Ca , and ^{48}Ca . In this study we extend these studies to $0\nu\beta\beta$ decays of medium-heavy and heavy nuclei by computing the average OMC matrix elements in the intermediate nuclei of $0\nu\beta\beta$ decays up to some 50 MeV

using the pnQRPA formalism and compare them with the energy-multipole decompositions of the NMEs of $0\nu\beta\beta$ decays computed using the same formalism and model spaces. We compute the average OMC matrix elements instead of OMC rates in order to reduce the phase-space effects. We decompose the average OMC ME to J^π multipole states within MeV energy bins while for the $0\nu\beta\beta$ decay the energy-multipole decomposition entails division of the NMEs into multipoles and their energy distributions binned by MeV energy intervals. In [23] we computed the strength functions for the OMC on ^{76}Se , ^{82}Kr , ^{96}Mo , ^{100}Ru , ^{116}Sn , ^{128}Xe , ^{130}Xe , and ^{136}Ba , leading to states in $0\nu\beta\beta$ intermediate nuclei ^{76}As , ^{82}Br , ^{96}Nb , ^{100}Tc , ^{116}In , ^{128}I , ^{130}I , and ^{136}Cs . In this study we extend those calculations by comparing the average OMC matrix elements with the corresponding energy-multipole decompositions of $0\nu\beta\beta$ NMEs.

Since we are interested in wide excitation-energy regions of medium-heavy or heavy open-shell nuclei, the shell-model framework is infeasible for our calculations due to the enormous computational burden and the very restricted single-particle model spaces allowed by the shell-model treatment. The pnQRPA formalism allows us to study the OMC and $0\nu\beta\beta$ decay NMEs at high excitation energies, since it allows the use of large no-core single-particle bases. Even though the pnQRPA often fails to predict the properties of individual states accurately, it can reproduce the gross features of a distribution of nuclear states quite reasonably. In our earlier studies, it has been shown that the pnQRPA reliably reproduces the locations of the isovector spin-dipole giant resonances [24], as well as the location of the newly discovered OMC giant resonance in the case of ^{100}Mo [25,26], and the low-energy OMC rates in the case of ^{76}Se [1,23].

This article is organized as follows. In Sec. II we briefly introduce the pnQRPA formalism as well as the underlying formalism of the ordinary muon capture and $0\nu\beta\beta$ decay. In Sec. III we display and discuss the obtained results for the OMC rates and $0\nu\beta\beta$ -decay matrix elements and examine possible connections between them. The final conclusions are drawn in Sec. IV.

II. COMPUTATIONAL SCHEME

In this section we introduce briefly our computational scheme. All the calculations are based on the pnQRPA theory. In the first subsection we outline the key points of the pnQRPA theory and introduce the parameters related to the corresponding Hamiltonian. In the second subsection we outline the theoretical aspects of the OMC rate, and in the last subsection we introduce the underlying theory of the $0\nu\beta\beta$ -decay NMEs.

A. pnQRPA and its Hamiltonian parameters

For the present calculations we adopt the spherical version of the proton-neutron QRPA. The calculations use an even-even nucleus as a reference and then create proton-neutron excitations to reach the states of the adjacent odd-odd nucleus. We find the wave functions and excitation energies for the complete set of J^π excitations in the odd-odd nuclei by performing a pnQRPA diagonalization in the unperturbed basis

of quasiproton-quasineutron pairs coupled to J^π [27,28]. The resulting pnQRPA states in odd-odd nuclei are of the form

$$|J_k^\pi M\rangle = \sum_{pn} [X_{pn}^{J_k^\pi} A_{pn}^\dagger(JM) - Y_{pn}^{J_k^\pi} \tilde{A}_{pn}(JM)] |\text{pnQRPA}\rangle, \quad (3)$$

where k labels the states of spin-parity J^π , the quantities X and Y are the forward- and backward-going pnQRPA-amplitudes, A^\dagger and \tilde{A} are the quasiproton-quasineutron creation and annihilation operators, M is the z projection of J and $|\text{pnQRPA}\rangle$ is the pnQRPA vacuum. The transition densities corresponding to transitions between the 0_{gs}^+ ground state of the even-even reference nucleus and a J_k^π excited state of the corresponding odd-odd nucleus, entering both the muon capture rates and the $0\nu\beta\beta$ NMEs, can then be written as

$$\langle 0_{\text{gs}}^+ || [c_p^\dagger \tilde{c}_n]_J || J_k^\pi \rangle = \sqrt{2J+1} [v_p u_n X_{pn}^{J_k^\pi} + u_p v_n Y_{pn}^{J_k^\pi}], \quad (4)$$

$$\langle J_k^\pi || [c_p^\dagger \tilde{c}_n]_J || 0_{\text{gs}}^+ \rangle = \sqrt{2J+1} [u_p v_n X_{pn}^{J_k^\pi} + v_p u_n Y_{pn}^{J_k^\pi}], \quad (5)$$

where v (u) is the BCS occupation (vacancy) amplitude in the even-even nucleus. The formalism is explained in more detail in Refs. [27,28].

The X and Y amplitudes in Eq. (3) are calculated by diagonalizing the pnQRPA matrix separately for each multipole J^π . We adopt as the two-body interaction the one derived from the Bonn-A one-boson-exchange potential, introduced in [29]. We follow the partial isospin-restoration scheme introduced in [30], and multiply the isoscalar ($T=0$) and isovector ($T=1$) parts of the particle-particle G -matrix elements by factors $g_{\text{pp}}^{T=0}$ and $g_{\text{pp}}^{T=1}$, respectively. The isovector parameter $g_{\text{pp}}^{T=1}$ is adjusted such that the Fermi part of the corresponding two-neutrino double beta ($2\nu\beta\beta$) NME vanishes, leading to partial isospin-symmetry restoration. The isoscalar parameter $g_{\text{pp}}^{T=0}$ is subsequently varied to reproduce the $2\nu\beta\beta$ -decay half-life. As for the particle-hole part, it was scaled by a common factor g_{ph} , fixed, as usual, by fitting the centroid of the Gamow-Teller giant resonance (GTGR) in the 1^+ channel of the calculations. These (particle-particle and particle-hole) renormalization factors are adopted from [24] except for the case $A=82$, which was not included in there. For $A=82$ we adopt the values from [23].

The quasiparticle spectra for protons and neutrons, needed in the pnQRPA diagonalization, are obtained by solving the BCS equations for protons and neutrons in the even-even reference nuclei. The calculated BCS pairing gaps are fitted to the phenomenological proton and neutron pairing gaps in a way described in detail in [31]. The values of the resulting pairing scaling factors are listed in [24,31].

For each even-even reference nucleus involved in the computations, we adopt the single-particle bases exploited successfully in our earlier calculations [23,24,31], i.e., we employ no-core bases with all the orbitals from the $N=0$ oscillator major shell up to at least two oscillator major shells above the respective Fermi surfaces for both protons and neutrons. The single-particle energies were obtained by solving the radial Schrödinger equation for a Coulomb-corrected Woods-Saxon (WS) potential, optimized for nuclei close to the β -stability line [32]. As was mentioned in [24,31], this choice is justified since the $\beta\beta$ -decaying nuclei are always situated rather close

to the bottom of the valley of beta stability. Both the bound and quasi-bound single-particle states are taken along in the calculations. The single-particle energies close to the Fermi surfaces were slightly modified in order to better reproduce the low-lying spectra of the neighboring odd-mass nuclei at the BCS-quasiparticle level.

B. Formalism of the ordinary muon capture

We compute the OMC nuclear matrix elements and rates using the formalism that was originally developed by Morita and Fujii in [33]. This formalism takes into account both the genuine and induced vector and axial-vector weak nucleon currents. The OMC rate from a J_i initial state to a J_f final state can be written as

$$W = 2\pi \langle |\text{M.E.}|^2 \rangle_{av} q^2 \frac{dq}{dE_f}, \quad (6)$$

where

$$\frac{dq}{dE_f} = \left[1 - \frac{q}{m_\mu + AM} \right] \quad (7)$$

and

$$\begin{aligned} \langle |\text{M.E.}|^2 \rangle_{av} &= \frac{2J_f + 1}{(2j' + 1)(2J_i + 1)} \sum_{ij} \sum_{\kappa u} \\ &\times \left[\sum_v C^{(i)} \mathcal{M}_{vu}^{(i)} \right]^* \left[\sum_{v'} C^{(j)} \mathcal{M}_{v'u}^{(j)} \right], \quad (8) \end{aligned}$$

where j' is the angular momentum of the bound muon. The definitions of the matrix elements $\mathcal{M}_{vu}^{(i)}$ and the corresponding coefficients $C^{(i)}$ can be found in Table I of [33].

The Q value of the OMC process can be computed from

$$q = (m_\mu - W_0) \left(1 - \frac{m_\mu - W_0}{2(M_f + m_\mu)} \right), \quad (9)$$

where $W_0 = M_f - M_i + m_e + E_X$ [33]. Here, M_f (M_i) is the nuclear mass of the final (initial) nucleus, m_e the rest mass of an electron, and E_X the excitation energy of the final J^π state.

If we assume that the muon is initially bound on the K atomic orbit, and use Bethe-Salpeter point-like-nucleus approximation formula [34] for the bound muon wave function, the capture rate of Eq. (6) can be written as

$$W = 8P(\alpha Z m'_\mu)^3 \frac{2J_f + 1}{2J_i + 1} \left(1 - \frac{q}{m_\mu + AM} \right) q^2, \quad (10)$$

where A is the mass number of the initial and final nuclei, J_i (J_f) the angular momentum of the initial (final) nucleus, M the average nucleon rest mass, m_μ the mass of the bound muon, m'_μ the reduced mass of the muon in the parent μ -mesonic atom, Z the atomic number of the initial nucleus, α the fine-structure constant, and q the decay energy (Q value) of the OMC.

The term P in Eq. (10) has a complex form containing the nuclear matrix elements of the OMC, various geometric and kinematic factors, and weak coupling constants. The P term can be written explicitly for an n th forbidden transition. In [33] the authors derive explicit forms for the P term for different degrees of forbiddenness, assuming the muon being bound

on the atomic K orbit before capture, and approximating the bound-state muon wave function as the one of a point nucleus. All terms of the order of $1/M^2$ (except for terms containing the square of the weak pseudoscalar coupling, g_P , which is large compared with the other coupling constants) were omitted. We extend these explicit forms by including all the terms of the order of $1/M^2$ in our calculations, as given explicitly in [23].

The P term involves the usual weak vector and axial-vector couplings $g_V \equiv g_V(q)$ and $g_A \equiv g_A(q)$ at finite momentum transfer $q > 0$. The conserved vector current (CVC) and partially conserved axial-vector current (PCAC) hypotheses give the values $g_V(0) = 1.00$ and $g_A(0) = 1.27$ for a free nucleon at zero momentum transfer, and for finite momentum transfer we can use the dipole approximation [2]. For the induced pseudoscalar coupling g_P the Goldberger-Treiman PCAC relation [35] gives $g_P/g_A = 7.0$. However, deviations from the CVC and PCAC values have been recorded at zero momentum transfer [7,8,22,36].

Using the notation of Eq. (10) we can write Eq. (8) in the form

$$\langle |\text{M.E.}|^2 \rangle_{av} = \frac{8(2J_f + 1)}{2J_i + 1} (\alpha Z m'_\mu)^3 P. \quad (11)$$

Here, we define an average OMC matrix element as

$$|M^{(\mu)}|_{av} = \sqrt{\langle |\text{M.E.}|^2 \rangle_{av}} = \sqrt{\frac{8(2J_f + 1)}{2J_i + 1} (\alpha Z m'_\mu)^3 P}. \quad (12)$$

We compare this quantity, instead of OMC rate, with the $0\nu\beta\beta$ decay nuclear matrix element in order to reduce the phase-space effects.

In this work we choose the slightly quenched values of $g_A(0) = 0.8$ and $g_P(0) = 7.0$ and keep the CVC value $g_V(0) = 1.00$ for all the studied cases. These values were adopted also in our earlier works [23,26] but the (qualitative) results of the present study are not sensitive to the exact values of these couplings.

C. Outline of the $0\nu\beta\beta$ -decay theory

We exploit the $0\nu\beta\beta$ -decay formalism outlined, e.g., in [37] and further processed in [24,38], assuming that the $0\nu\beta\beta$ decay is dominated by the light-Majorana-neutrino-exchange mechanism. Here, we are only interested in the ground-state-to-ground-state transitions. The half-life for such a $0\nu\beta\beta$ transition can be written as

$$[t_{1/2}^{(0\nu)}(0_i^+ \rightarrow 0_f^+)]^{-1} = (g_A^{\text{eff}})^4 G_{0\nu} |M^{(0\nu)}|^2 \left| \frac{\langle m_\nu \rangle}{m_e} \right|^2, \quad (13)$$

where $G_{0\nu}$ is a phase-space factor for the final-state leptons in units of inverse years (see [39]), defined here without including the axial-vector coupling g_A . The effective light-neutrino mass, $\langle m_\nu \rangle$, of Eq. (13) is defined as

$$\langle m_\nu \rangle = \sum_j (U_{ej})^2 m_j \quad (14)$$

with m_j being the mass eigenstates of light neutrinos. The amplitudes U_{ej} are the components of the electron row of the light-neutrino-mass mixing matrix.

The $0\nu\beta\beta$ -decay NME $M^{(0\nu)}$ in Eq. (13) is defined as

$$M^{(0\nu)} = M_{\text{GT}}^{(0\nu)} - \left(\frac{g_V}{g_A^{\text{eff}}}\right)^2 M_{\text{F}}^{(0\nu)} + M_{\text{T}}^{(0\nu)}, \quad (15)$$

where we adopt the CVC value $g_V = 1.0$ for the weak vector coupling strength. The double Fermi, Gamow-Teller, and tensor nuclear matrix elements for $0\nu\beta\beta$ decays are defined as

$$M_{\text{F}}^{(0\nu)} = \sum_k \left(0_f^+ \parallel \sum_{mn} h_{\text{F}}(r_{mn}, E_k) t_m^- t_n^- \parallel 0_i^+ \right), \quad (16)$$

$$M_{\text{GT}}^{(0\nu)} = \sum_k \left(0_f^+ \parallel \sum_{mn} h_{\text{GT}}(r_{mn}, E_k) (\boldsymbol{\sigma}_m \cdot \boldsymbol{\sigma}_n) t_m^- t_n^- \parallel 0_i^+ \right), \quad (17)$$

$$M_{\text{T}}^{(0\nu)} = \sum_k \left(0_f^+ \parallel \sum_{mn} h_{\text{T}}(r_{mn}, E_k) S_{mn}^{\text{T}} t_m^- t_n^- \parallel 0_i^+ \right), \quad (18)$$

where t_m^- is the isospin lowering operator (changing a neutron into a proton) for the nucleon m . The spin tensor operator S_{mn}^{T} is defined as

$$S_{mn}^{\text{T}} = 3[(\boldsymbol{\sigma}_m \cdot \hat{\mathbf{r}}_{mn})(\boldsymbol{\sigma}_n \cdot \hat{\mathbf{r}}_{mn})] - \boldsymbol{\sigma}_m \cdot \boldsymbol{\sigma}_n. \quad (19)$$

The summation over k in Eqs. (16)–(18) runs over all the states of the intermediate odd-odd nucleus, and E_k is the excitation energy of a given state. Here, $r_{mn} = |\mathbf{r}_m - \mathbf{r}_n|$ is the relative distance between the two decaying neutrons, labeled m and n , and $\hat{\mathbf{r}}_{mn} = (\mathbf{r}_m - \mathbf{r}_n)/r_{mn}$. The ground state of the initial (final) even-even nucleus is denoted by 0_i^+ (0_f^+). The terms $h_K(r_{mn}, E_k)$, $K = \text{F, GT, T}$ are the neutrino potentials defined in [38].

In the pnQRPA framework the nuclear matrix elements can be written as

$$\begin{aligned} M_K^{(0\nu)} &= \sum_{J^\pi, k_1, k_2, J'} \sum_{pp'nn'} (-1)^{j_n + j_{p'} + J + J'} \sqrt{2J' + 1} \\ &\times \left\{ \begin{matrix} j_p & j_n & J \\ j_{n'} & j_{p'} & J' \end{matrix} \right\} (pp'; J' \parallel \mathcal{O}_K \parallel nn'; J') \\ &\times (0_f^+ \parallel [c_p^\dagger \tilde{c}_n]_J \parallel |J_{k_1}^\pi \rangle \langle J_{k_2}^\pi| |J_{k_2}^\pi \rangle \parallel [c_p^\dagger \tilde{c}_n]_J \parallel 0_i^+), \end{aligned} \quad (20)$$

where the summation over k_1 and k_2 runs over the different pnQRPA solutions for a given multipole J^π . The operators \mathcal{O}_K inside the two-particle matrix element refer to Eqs. (16)–(18), and they can be written as

$$\mathcal{O}_{\text{F}} = h_{\text{F}}(r, E_k) [f_{\text{CD}}(r)]^2, \quad (21)$$

$$\mathcal{O}_{\text{GT}} = h_{\text{GT}}(r, E_k) [f_{\text{CD}}(r)]^2 \boldsymbol{\sigma}_1 \boldsymbol{\sigma}_2, \quad (22)$$

$$\mathcal{O}_{\text{T}} = h_{\text{T}}(r, E_k) [f_{\text{CD}}(r)]^2 S_{12}^{\text{T}}, \quad (23)$$

where S_{12}^{T} is the tensor operator of Eq. (19) and $r = |\mathbf{r}_1 - \mathbf{r}_2|$ is the distance between the participating nucleons. The energy E_k is the average of the k th pnQRPA-computed eigenvalues of the initial and final nuclei, corresponding to a given multipole J^π . The term $\langle J_{k_1}^\pi | J_{k_2}^\pi \rangle$ is the overlap between the two sets of

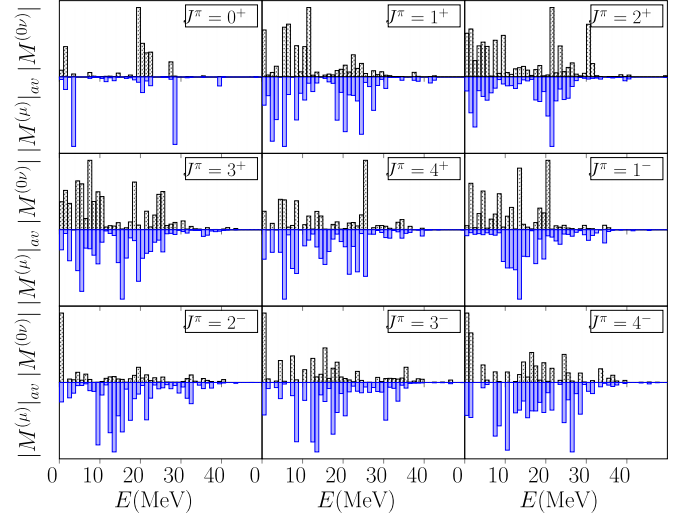


FIG. 1. Multipole decompositions in terms of relative $0\nu\beta\beta$ matrix elements (positive y axes) and average matrix elements of the OMC on ^{76}Se (negative y axes) as functions of the excitation energy E in the intermediate nucleus ^{76}As of the $0\nu\beta\beta$ decay of ^{76}Ge . Here, J^π refer to the angular momenta and parities of the virtual states in ^{76}As and all quantities have been summed within 1 MeV energy bins. The scale values of the y axes have been omitted, since they are not relevant for the current analysis. For more information see the text.

J^π states, and it can be written as

$$\langle J_{k_1}^\pi | J_{k_2}^\pi \rangle = \sum_{pn} [X_{pn}^{J_{k_1}^\pi} \bar{X}_{pn}^{J_{k_2}^\pi} - Y_{pn}^{J_{k_1}^\pi} \bar{Y}_{pn}^{J_{k_2}^\pi}], \quad (24)$$

where X and Y (\bar{X} and \bar{Y}) are the pnQRPA amplitudes of the final (initial) nucleus.

The factor $f_{\text{CD}}(r)$ in Eqs. (21)–(23) takes into account the nucleon-nucleon short-range correlations (SRC) [40,41]. We use the CD-Bonn form [42] with the parametrization

$$f_{\text{CD}}(r) = 1 - 0.46e^{-(1.52/\text{fm}^2)r^2} [1 - (1.88/\text{fm}^2)r^2]. \quad (25)$$

III. RESULTS AND DISCUSSION

In this section we present and discuss the results of our studies. We concentrate on the positive $J^\pi = 0^+, 1^+, 2^+, 3^+, 4^+$ and negative $J^\pi = 1^-, 2^-, 3^-, 4^-$ multiplicities of both the average OMC ME distributions and the $0\nu\beta\beta$ NME distributions. These multipoles are by far the most important ones for the OMC rates [23] and the leading ones for the $0\nu\beta\beta$ NMEs [24,43]. We discuss also the cumulative average OMC MEs and $0\nu\beta\beta$ NMEs.

We computed the average OMC MEs and the $0\nu\beta\beta$ -decay NMEs using the formalism and parameters discussed in Sec. II A. For the values of the weak coupling constants, involved in both the $0\nu\beta\beta$ and OMC processes, we adopt the moderately quenched values $g_A = 0.8$ and $g_P = 7.0$, and the CVC value $g_V = 1.0$. This is in line with our earlier studies [23,26]. As stated at the end of Sec. II B, the results are not very sensitive to the values of these couplings.

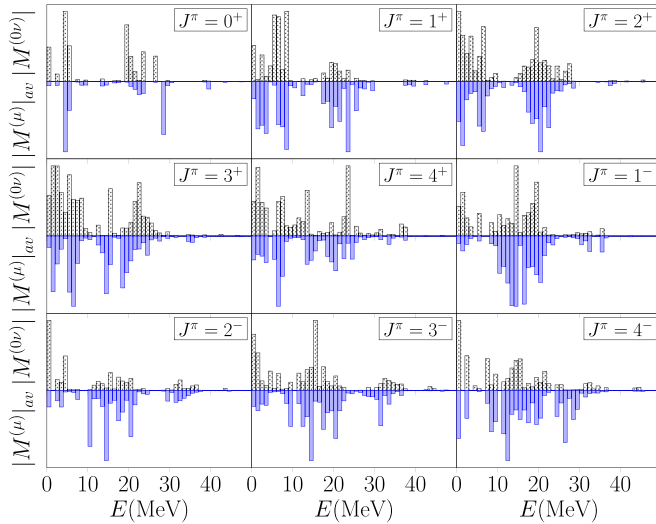


FIG. 2. The same as in Fig. 1 for the $A = 82$ system.

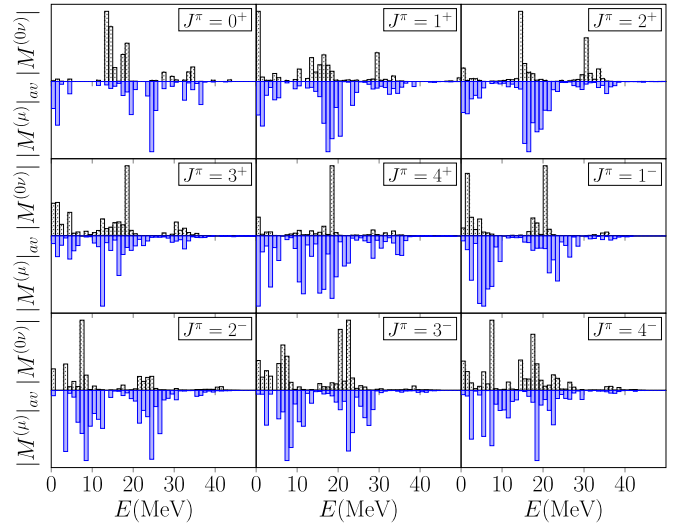


FIG. 5. The same as in Fig. 1 for the $A = 116$ system.

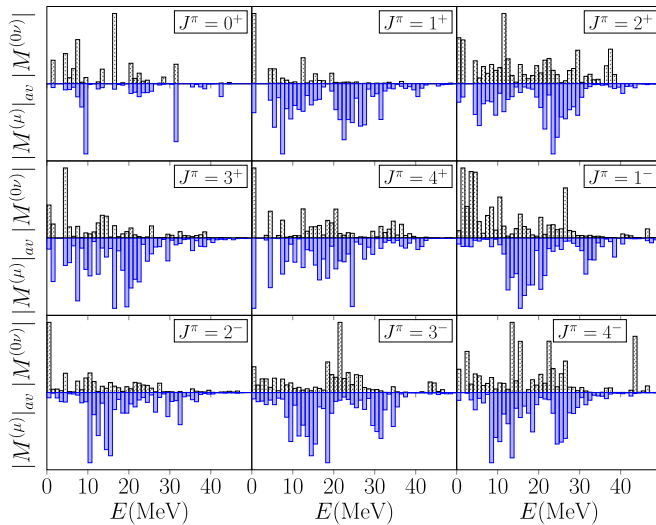


FIG. 3. The same as in Fig. 1 for the $A = 96$ system.

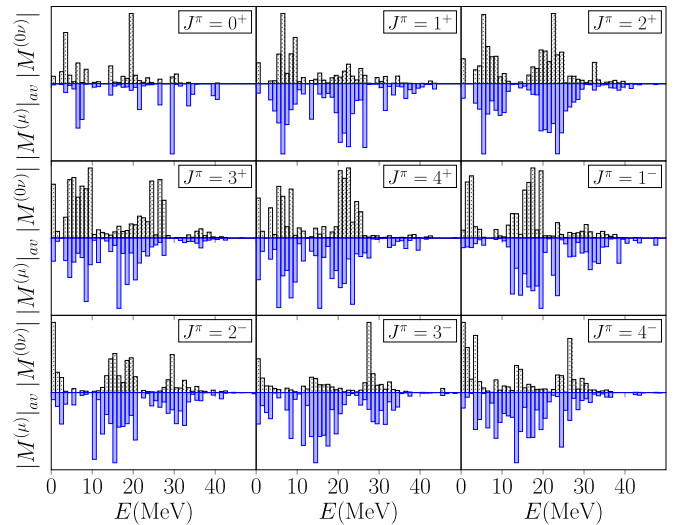


FIG. 6. The same as in Fig. 1 for the $A = 128$ system.

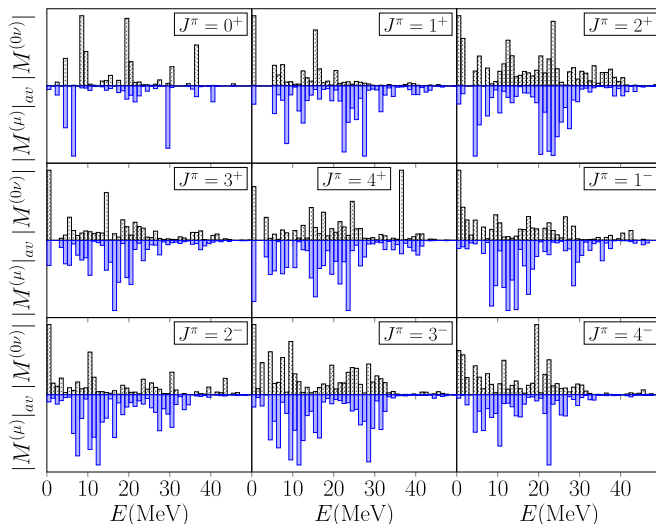


FIG. 4. The same as in Fig. 1 for the $A = 100$ system.

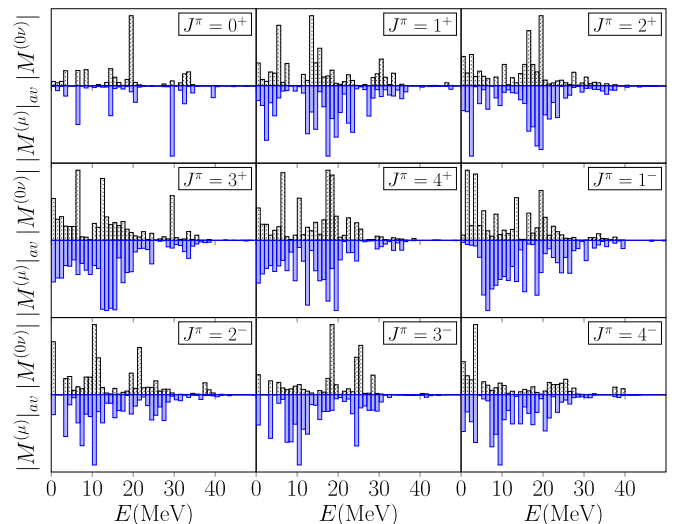
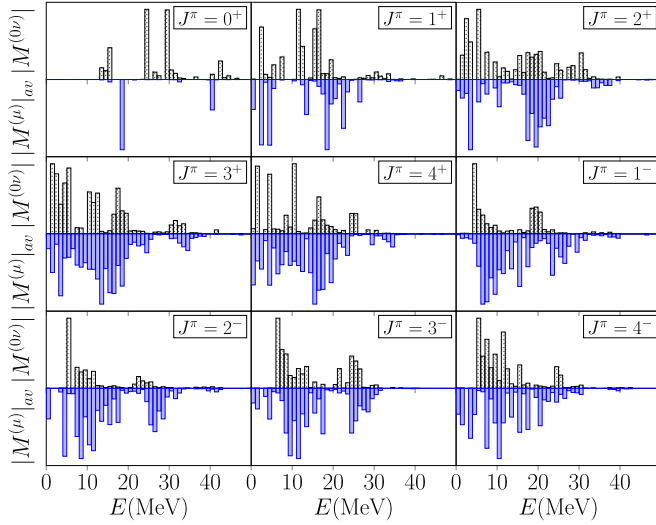


FIG. 7. The same as in Fig. 1 for the $A = 130$ system.

FIG. 8. The same as in Fig. 1 for the $A = 136$ system.

A. Distributions of the relative OMC MEs and $0\nu\beta\beta$ NMEs

In Figs. 1–8 we compare the computed relative OMC ME distributions

$$|M^{(\mu)}|_{av}(J^\pi)(E) / \sum_E |M^{(\mu)}|_{av}(J^\pi)(E)$$

with the multipole decompositions $M^{(0\nu)}(J^\pi)$ of the $0\nu\beta\beta$ -decay NMEs expressed in terms of relative contributions

$$|M^{(0\nu)}(J^\pi)|(E) / \sum_E |M^{(0\nu)}(J^\pi)|(E).$$

The analyses have been done for each multipole J^π separately, and for increasing excitation energy E in the OMC daughter (the same as $0\nu\beta\beta$ -decay intermediate nucleus) using summed average OMC MEs and $0\nu\beta\beta$ NMEs within energy bins of 1 MeV. We have chosen to plot only absolute values of the matrix elements since they carry the essential information needed in the present comparison of the OMC and $0\nu\beta\beta$ decay. Only in the case of $A = 100$ the $J^\pi = 1^+$ contribution to the total $0\nu\beta\beta$ NME is negative. There are, however, negative contributions coming from individual energy bins in many cases (the same is of course true for the OMC matrix element). As such, the possible different relative signs of the contributions are not important in the context of our study, since we are interested in the multipoles and energy regions where notable (positive or negative) contributions appear in both the OMC matrix element and the $0\nu\beta\beta$ NME. This means that the nuclear states, with their wave functions, play an important role in both processes for these particular multipoles and energy regions. In order to make the comparison meaningful the excitation energy of the lowest J^π state of the pnQRPA set (for $0\nu\beta\beta$ decay the right-hand set) is fitted to the measured excitation energy. We display the relative $0\nu\beta\beta$ multipole NMEs on the positive and relative OMC MEs on the negative y axes. Since the comparison is qualitative and the quantities are relative we have omitted the scales of the y axes.

In the following we analyze the correspondences related to different multipoles arising from the Figs. 1–8. It should be noted that the number of 0^+ pnQRPA states is little, and hence the similarities between the two distributions are harder to conclude than for the other multipoles.

A = 76: The correspondence between relative OMC-rate and $0\nu\beta\beta$ -NME distributions for the multipoles $J^\pi = 0^+$ is weak. However, for the rest of the multipoles one can see correspondences: in the cases of $J^\pi = 1^+, 2^+, 3^+$ one can see two bumps at similar energies. The $J^\pi = 1^-$ distributions both are peaked at ≈ 10 MeV, and the $J^\pi = 3^-, 4^-$ distributions at ≈ 15 MeV. On the other hand, in the case of $J^\pi = 2^-$ the $0\nu\beta\beta$ decays through the 2^- ground state of ^{76}As seem to be enhanced.

A = 82: The $J^\pi = 1^+, 2^+, 3^+$ and $J^\pi = 1^-, 3^-$ distributions show nice correspondence. The $J^\pi = 0^+$ distributions both show a peak at $E \approx 5$ MeV, and the low-energy correspondences of $J^\pi = 4^\pm$ are also pretty good. In the case of $J^\pi = 2^-$ $0\nu\beta\beta$ seems to be more concentrated in low

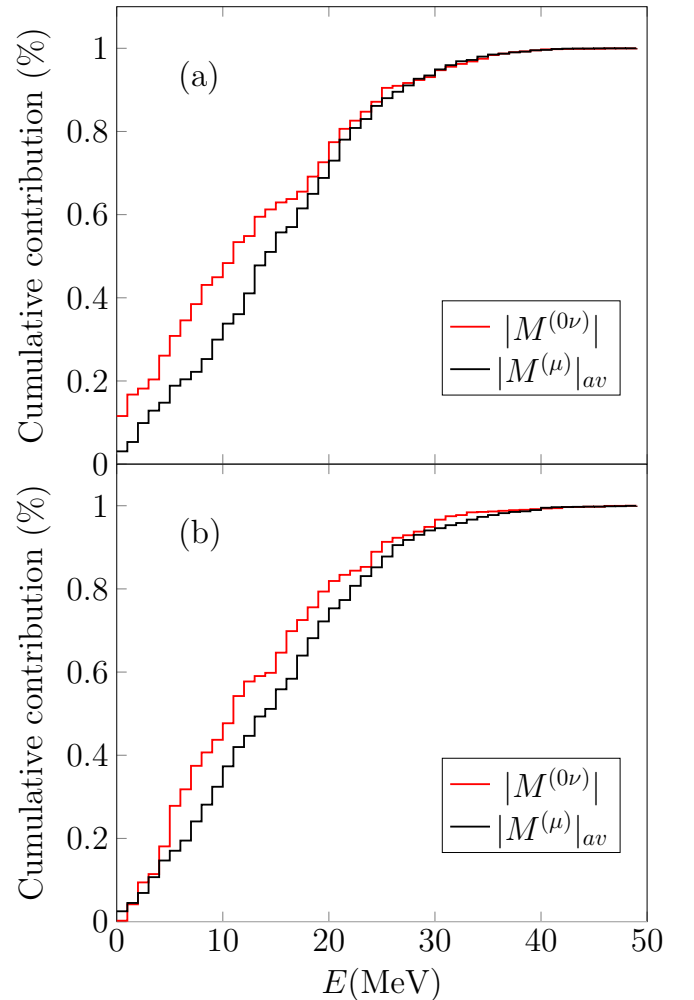


FIG. 9. Normalized cumulative average OMC MEs and normalized $0\nu\beta\beta$ NMEs as functions of energy in the intermediate nuclei ^{76}As (a) and ^{136}Cs (b) of the $A = 76$ and $A = 136$ $0\nu\beta\beta$ triplets. For more information, see the text.

TABLE I. Contributions (in percentages) from different multipoles to $0\nu\beta\beta$ -decay NMEs and average OMC MEs for different $0\nu\beta\beta$ -decay triplets. The presented values are normalized ratios $R(0\nu) = |M^{(0\nu)}(J^\pi)|/|M^{(0\nu)}|$ and $R(\mu) = |M^{(\mu)}|_{av}(J^\pi)/|M^{(\mu)}|_{av}$.

Case J^π	A = 76		A = 82		A = 96		A = 100		A = 116		A = 128		A = 130		A = 136	
	$R(0\nu)$	$R(\mu)$														
0^+	2	3	2	2	0	3	1	2	1	2	1	3	1	2	1	2
1^+	7	18	6	17	6	17	6	17	9	16	2	16	2	14	7	14
1^-	16	21	16	21	18	18	20	19	23	18	13	17	13	17	9	17
2^+	13	16	14	17	13	16	12	16	9	16	12	17	12	15	14	15
2^-	10	18	9	17	7	17	3	17	7	17	5	16	5	17	6	16
3^+	5	11	5	11	6	12	5	12	6	11	6	12	6	12	7	12
3^-	11	6	11	6	10	7	9	8	9	8	10	8	10	9	9	9
4^+	7	2	7	2	8	2	8	2	7	3	9	3	9	4	9	4
4^-	5	5	5	5	4	5	4	5	4	5	5	5	5	6	5	6
Σ	76	10	75	98	72	97	68	98	75	96	63	97	63	96	67	95

energies, but both distributions show three clear bumps at similar energies.

A = 96: The $J^\pi = 0^+$ distributions show three bumps at energies $E \approx 10, 20, 30$ MeV, but there is a strong peak in the $0\nu\beta\beta$ distribution at $E \approx 15$ MeV, that is missing from the OMC distribution. In the cases of $J^\pi = 1^+$ and $J^\pi = 2^-$ the $0\nu\beta\beta$ distributions are clearly more concentrated on lower energies than OMC. The correspondence of $J^\pi = 2^+, 3^+, 1^-$, and 3^- is not too good, either. However, the $J^\pi = 4^+$ distributions show three clear bumps at similar energies.

A = 100: In this case, the situation in the cases of $J^\pi = 1^\pm$ and 2^- is similar as in Figs. 3(b) and 3(g): $0\nu\beta\beta$ is more concentrated on lower energies. However, the $J^\pi = 2^+$ distributions both show a clear bump at $E \approx 25$ MeV, and $J^\pi = 3^+$ at $E \approx 15$ MeV. The $J^\pi = 4^+$ distributions show good correspondence at $E < 30$ MeV, but there is an extra peak at $E \approx 35$ MeV in the $0\nu\beta\beta$ distribution. The $J^\pi = 3^-, 4^-$, on the other hand, show two clear bumps at similar energies.

A = 116: In this case, the correspondence is best for the $J^\pi = 1^+, 2^+, 3^+$ multipoles, which show three clear bumps in both distributions. In the case of $J^\pi = 4^+$ there is some concentration in both distributions at around 20 MeV. There are similarities also in the cases of the $J^\pi = 1^-, 2^-, 3^-, 4^-$: there are two clear bumps at similar energies in both spectra. On the other hand, the $J^\pi = 0^+$ distributions show no clear correspondence.

A = 128: In this case, the correspondence is best for the $J^\pi = 1^+, 2^+, 3^+, 4^+$ and 4^- multipoles, which show two clear bumps at $E \approx 8$ MeV and at $E \approx 20$ MeV, and for $J^\pi = 1^-, 2^-, 3^-$, which show three bumps. The $J^\pi = 0^+$ distributions also have two peaks at $E \approx 5$ and 20 MeV.

A = 130: In this case, the low-energy correspondence for $J^\pi = 2^-, 4^-$ multipoles is great. The $J^\pi = 0^+, 1^+$ distributions both show three peaks, and the $J^\pi = 2^+, 3^+, 4^+$ three bumps at similar energies. The $J^\pi = 3^-$ distributions also show two bumps at $E \approx 10$ and 25 MeV, but there is an extra peak in the $0\nu\beta\beta$ distribution that is absent in the OMC distribution. In the case of $J^\pi = 1^-$ the $0\nu\beta\beta$ decay is more concentrated on lower energies.

A = 136: In this case, the correspondence is clearest for the $J^\pi = 1^+, 2^+$ distributions, which show two bumps at around $E \approx 3$ MeV and at $E \approx 20$ MeV. The $J^\pi = 3^-$ distributions also show two bumps at around $E \approx 10$ MeV and $E \approx 25$ MeV. As for the $J^\pi = 1^-, 2^-$ multipoles, there are two bumps in both distributions, but the second bump is situated at slightly lower energy for in the $0\nu\beta\beta$ distribution. In the case of $J^\pi = 4^-$ the OMC distribution is more spread compared to the $0\nu\beta\beta$ distribution, but both distributions show a bump at around $E \approx 10$ MeV.

All in all, the correspondence between the $J^\pi = 0^+$ $0\nu\beta\beta$ -NME and OMC-ME distributions seems to be not too good, and the overall correspondence seems to be best for the $J^\pi = 3^\pm$ and 4^\pm multipoles. Also for other multipoles there seems to be a more or less clear correspondence for all the discussed $0\nu\beta\beta$ triplets. The distributions and their correspondences vary quite much between the different $0\nu\beta\beta$ triplets indicating that nuclear structure varies strongly with nuclear mass owing to different mean-field properties (single-particle energies, Fermi surfaces) and two-nucleon correlations.

B. Cumulative average OMC MEs and $0\nu\beta\beta$ NMEs

Cumulative average OMC MEs and $0\nu\beta\beta$ NMEs nicely illustrate the build-up of these quantities as functions of the excitation energy in the intermediate nuclei of the discussed $0\nu\beta\beta$ triplets. We choose the $A = 76$ and $A = 136$ triplets as representative cases and plot the corresponding cumulative matrix elements

$$\sum_{J^\pi} |M^{(0\nu)}(J^\pi)|(E) / \sum_{J^\pi, E} |M^{(0\nu)}(J^\pi)|(E)$$

and

$$\sum_{J^\pi} |M^{(\mu)}|_{av}(J^\pi)(E) / \sum_{J^\pi, E} |M^{(\mu)}|_{av}(J^\pi)(E)$$

in Fig. 9. Thus, Fig. 9 is just an other way to present the results of Figs. 1–8. We can see that the running sums for the average OMC MEs and $0\nu\beta\beta$ NMEs, for both triplets, are quite similar, but in the $A = 76$ case [panel (a)] the $0\nu\beta\beta$

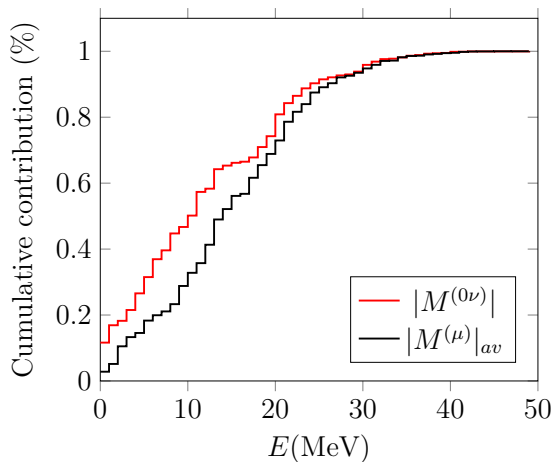


FIG. 10. The same as in Fig. 9, but only for the $A = 76$ $0\nu\beta\beta$ -decay triplet and containing contributions from only the leading multipoles $J^\pi = 1^+, 1^-, 2^+, 2^-$.

NME starts at a higher value and has thus a smaller inclination of the cumulative curve. Both cases show that $0\nu\beta\beta$ decay is slightly more concentrated on lower energies than OMC.

In Table I we show for the discussed $0\nu\beta\beta$ -decay triplets the relative multipole contributions to the $0\nu\beta\beta$ NMEs and average OMC MEs for $J^\pi (J \leq 4)$, which are the leading multipoles for both the $0\nu\beta\beta$ decay and OMC (see Figs. 1 and 3 of [38], and the results of [23]). The multipole $J^\pi = 0^-$ is omitted from the table, since its contribution to both $|M^{(0\nu)}|$ and $|M^{(\mu)}|_{av}$ is negligible. First of all, one can see that basically all of the OMC strength is coming from the multipoles with $J \leq 4$, while the $0\nu\beta\beta$ strength is more distributed to higher multipoles, and only about 60–75% comes from the multipoles with $J \leq 4$. Having a closer look at the table one notices that the multipoles $J^\pi = 1^+, 1^-, 2^+, 2^-$ are among the leading multipoles for both the $0\nu\beta\beta$ decay and OMC for all the nuclei. Also multipoles $J^\pi = 3^-, 4^+$ are important for the $0\nu\beta\beta$ NMEs, but less important for the OMC. On the other hand, $J^\pi = 3^+$ is rather important for OMC but not so important for $0\nu\beta\beta$ decay. The $J^\pi = 2^+$ and 1^- contributions are practically the same for both quantities. On the other hand, a considerable part of the OMC strength is coming from the multipoles $J^\pi = 1^+, 2^-$, but they are less important for the $0\nu\beta\beta$ -decay NMEs. These features of the $0\nu\beta\beta$ -decay NMEs were also recorded in [38], the small quantitative deviations from our results stemming from the much smaller single-particle bases employed there.

The multipoles $J^\pi = 1^+, 1^-, 2^+, 2^-$ are, according to Table I, the leading multipoles for both the average OMC MEs and $0\nu\beta\beta$ NMEs in our example case of $A = 76$. In Fig. 10 we plot for the $A = 76$ case the cumulative sums of the OMC rate ($|M^{(\mu)}|_{av}$) and $0\nu\beta\beta$ NME ($|M^{(0\nu)}|$) stemming only from these multipoles. We notice that the $0\nu\beta\beta$ decay strength is coming from lower energies than the OMC strength, as is also the case for the total multipole contributions in Fig. 9. Comparing Figs. 9 and 10 implies that the multipoles

$J^\pi = 1^\pm, 2^\pm$ not only constitute most of the $0\nu\beta\beta$ decay and OMC strength, but also define the energy distributions of the processes.

IV. SUMMARY AND CONCLUSIONS

In this work we computed the average matrix elements corresponding to the ordinary muon capture on the 0^+ ground states of ^{76}Se , ^{82}Kr , ^{96}Mo , ^{100}Ru , ^{116}Sn , ^{128}Xe , ^{130}Xe , and ^{136}Ba , which are the daughter nuclei of the eight $0\nu\beta\beta$ -decaying parent nuclei ^{76}Ge , ^{82}Se , ^{96}Zr , ^{100}Mo , ^{116}Cd , ^{128}Te , ^{130}Te , and ^{136}Xe . We compared these matrix elements with the corresponding $0\nu\beta\beta$ -decay nuclear matrix elements. The calculations were performed using the proton-neutron quasiparticle RPA with realistic two-body interactions and slightly modified no-core Woods-Saxon single-particle bases. We studied the cumulative behavior of the average OMC MEs and $0\nu\beta\beta$ NMEs and also presented multipole decompositions of the average OMC MEs and $0\nu\beta\beta$ -decay NMEs.

We found that there are correspondences especially between the $J^\pi = 3^\pm, 4^\pm$ $0\nu\beta\beta$ NMEs and average OMC MEs, and also for other multipoles there can be seen correspondences for all the studied $0\nu\beta\beta$ -decay triplets. Furthermore, we noticed that overall the cumulative behavior of the $0\nu\beta\beta$ NMEs and average OMC MEs is quite similar, but for $A \leq 128$ the $0\nu\beta\beta$ NME is more evenly distributed within the energy region of $E = 0\text{--}50$ MeV than the OMC ME. This difference is related to the different behavior of these two quantities at low excitation energies in the $0\nu\beta\beta$ -decay intermediate nuclei.

When studying the multipole decompositions of the $0\nu\beta\beta$ -decay NMEs and average OMC MEs we found that basically all of the OMC strength is coming from the multipoles with $J \leq 4$, while the $0\nu\beta\beta$ strength is more distributed to higher multipoles, only approximately 60–75% coming from the multipoles with $J \leq 4$. We also found that the multipoles $J^\pi = 1^+, 2^+, 1^-, 2^-$ are among the leading multipoles for both the $0\nu\beta\beta$ decay and average OMC MEs for all the studied $0\nu\beta\beta$ -decay triplets.

According to this study, the overall behavior of the OMC and $0\nu\beta\beta$ matrix elements is pretty similar. Therefore, measurements of the OMC strength functions for the daughter nuclei of $0\nu\beta\beta$ decays could enable a systematic study of the involved nuclear wave functions and the sensitivity of the OMC strength functions to the effective values of the weak axial couplings, and hence help improve the accuracy of calculations of the NMEs of the $0\nu\beta\beta$ decay. Experimental studies are in progress, e.g., at RCNP Osaka for nuclei of interest in studies of nuclear double beta decay and astroneutrino interactions.

ACKNOWLEDGMENT

This work has been partially supported by the Academy of Finland under the Academy Project No. 318043.

- [1] D. Zinatulina, V. Brudanin, V. Egorov, C. Petitjean, M. Shirchenko, J. Suhonen, and I. Yutlandov, *Phys. Rev. C* **99**, 024327 (2019).
- [2] H. Ejiri, J. Suhonen, and K. Zuber, *Phys. Rep.* **797**, 1 (2019).
- [3] D. F. Measday, *Phys. Rep.* **354**, 243 (2001).
- [4] M. Kortelainen and J. Suhonen, *Europhys. Lett.* **58**, 666 (2002).
- [5] M. Kortelainen and J. Suhonen, *Nucl. Phys. A* **713**, 501 (2003).
- [6] M. Kortelainen and J. Suhonen, *J. Phys. G: Nucl. Part. Phys.* **30**, 2003 (2004).
- [7] E. Kolbe, K. Langanke, and P. Vogel, *Phys. Rev. C* **50**, 2576 (1994).
- [8] B. L. Johnson *et al.*, *Phys. Rev. C* **54**, 2714 (1996).
- [9] T. P. Gorringer *et al.*, *Phys. Rev. C* **60**, 055501 (1999).
- [10] T. Siiskonen, J. Suhonen, and M. Hjorth-Jensen, *J. Phys. G: Nucl. Part. Phys.* **25**, L55 (1999).
- [11] T. Siiskonen, M. Hjorth-Jensen, and J. Suhonen, *Phys. Rev. C* **63**, 055501 (2001).
- [12] N. Auerbach and B. A. Brown, *Phys. Rev. C* **65**, 024322 (2002).
- [13] F. Šimkovic, G. Pantis, J. D. Vergados, and A. Faessler, *Phys. Rev. C* **60**, 055502 (1999).
- [14] T. P. Gorringer *et al.*, *Phys. Rev. Lett.* **72**, 3472 (1994).
- [15] G. Jonkmans, S. Ahmad, D. S. Armstrong, G. Azuelos, W. Bertl, M. Blecher *et al.*, *Phys. Rev. Lett.* **77**, 4512 (1996).
- [16] D. Gazit, *Phys. Lett. B* **666**, 472 (2008).
- [17] L. E. Marcucci, A. Kievsky, S. Rosati, R. Schiavilla, and M. Viviani, *Phys. Rev. Lett.* **108**, 052502 (2012).
- [18] V. Brudanin *et al.*, *Nucl. Phys. A* **587**, 577 (1995).
- [19] T. Siiskonen, J. Suhonen, V. A. Kuz'min, and T. V. Tetereva, *Nucl. Phys. A* **635**, 446 (1998); **651**, 437(E) (1999).
- [20] T. Siiskonen, J. Suhonen, and M. Hjorth-Jensen, *Phys. Rev. C* **59**, R1839(R) (1999).
- [21] T. Gorringer and H. W. Fearing, *Rev. Mod. Phys.* **76**, 31 (2004).
- [22] J. Suhonen, *Front. Phys.* **5**, 55 (2017).
- [23] L. Jokiniemi and J. Suhonen, *Phys. Rev. C* **100**, 014619 (2019).
- [24] L. Jokiniemi, H. Ejiri, D. Frekers, and J. Suhonen, *Phys. Rev. C* **98**, 024608 (2018).
- [25] I. H. Hashim, H. Ejiri, T. Shima, K. Takahisa, A. Sato, Y. Kuno, K. Ninomiya, N. Kawamura, and Y. Miyake, *Phys. Rev. C* **97**, 014617 (2018).
- [26] L. Jokiniemi, J. Suhonen, H. Ejiri, and I. H. Hashim, *Phys. Lett. B* **794**, 143 (2019).
- [27] J. Suhonen, *From Nucleons to Nucleus: Concepts of Microscopic Nuclear Theory* (Springer, Berlin, 2007).
- [28] J. Suhonen, T. Taigel, and A. Faessler, *Nucl. Phys. A* **486**, 91 (1988).
- [29] K. Holinde, *Phys. Rep.* **68**, 121 (1981).
- [30] F. Šimkovic, V. Rodin, A. Faessler, and P. Vogel, *Phys. Rev. C* **87**, 045501 (2013).
- [31] L. Jokiniemi and J. Suhonen, *Phys. Rev. C* **96**, 034308 (2017).
- [32] A. Bohr and B. R. Mottelson, *Nuclear Structure, Vol. I* (Benjamin, New York, 1969).
- [33] M. Morita and A. Fujii, *Phys. Rev.* **118**, 606 (1960).
- [34] H. A. Bethe and E. E. Salpeter, *Quantum Mechanics of One- and Two-Electron Atoms* (Academic Press, New York, 1959).
- [35] M. L. Goldberger and S. B. Treiman, *Phys. Rev.* **111**, 354 (1958).
- [36] H. Ejiri, *Front. Phys.* **7**, 30 (2019).
- [37] J. Suhonen and O. Civitarese, *Phys. Rep.* **300**, 123 (1998).
- [38] J. Hyvärinen and J. Suhonen, *Phys. Rev. C* **91**, 024613 (2015).
- [39] J. Kotila and F. Iachello, *Phys. Rev. C* **85**, 034316 (2012).
- [40] G. A. Miller and J. E. Spencer, *Ann. Phys. (NY)* **100**, 562 (1976).
- [41] M. Kortelainen, O. Civitarese, J. Suhonen, and J. Toivanen, *Phys. Lett. B* **647**, 128 (2007).
- [42] F. Šimkovic, A. Faessler, H. Mütter, V. Rodin, and M. Stauf, *Phys. Rev. C* **79**, 055501 (2009).
- [43] J. Hyvärinen and J. Suhonen, *Adv. High Energy Phys.* **2016**, 4714829 (2016).